Proceedings of the 11th ICPMG 2026
11th International Conference on Physical Modelling in Geotechnics
8-12 June 2026, Zurich, Switzerland

Microfluidic investigation on similarity scaling principle of two-phase displacement in porous media under gravitational effect

Wenyuan Wang
Zhejiang University, Hangzhou, China, wenyuan.wang@zju.edu.cn

Bate Bate
Zhejiang University, Hangzhou, China, batechina@zju.edu.cn

Pengfei Liu
Zhejiang University, Hangzhou, China, pengf.liu@zju.edu.cn

ABSTRACT: To investigate and validate gravitational scaling of two phase displacement, experiments based on microfluidic apparatus are deployed in this study, utilizing microfluidic chips with pillars uniformly arranged in a triangular pattern as idealized porous media. Chips of two sizes are designed and fabricated according to scaling law derived theoretically, enabling direct observation of two-phase displacement processes. Bulk flow characteristics, including flow patterns, displacement efficiency fractal dimension, and breakthrough time are analysed to assess adherence to similarity. The results corroborate the theoretical scaling framework while revealing the gravitational effect in governing temporal and spatial scaling of displacement processes. These findings advance fundamental understanding of multiphase flow similarity and provide insights for hypergravity-assisted physical modelling in geotechnical and reservoir engineering applications.

1 ABSTRACT

Scaled physical modelling experiment remains an indispensable methodology for investigating diverse phenomena and dynamic processes, including slope stability, sediment transport, and thermal convection in fluids (Dai & Santamarina, 2017; Hawlader et al., 2008; Condie & Rhines, 1994; Girolami & Risso, 2020; Thring, 1953; Tong et al., 2017; L. Wang et al., 2019). While hypergravity can restore the gravitational stress gradient in scaled geotechnical models, it perturb multiphase flow dynamics within porous media—an effect particularly pronounced at elevated Bond numbers (Løvoll et al., 2005; Rücker et al., 2015). The variation of displacement pattern induced by gravitational effect may change the phase distribution in porous medium (Almajid & Abu-Al-Saud, 2022; Cui et al., 2019; Ewing & Berkowitz, 1998; Golmohammadi et al., 2021; Løvoll et al., 2005) , affect capillary force and ultimately compromise the similarity between scaled models and their full-scale prototypes.

Forcing on the two phase displacement, this study tends to investigate the gravitational effects and similarity relations via microfluidic experiments. The theoretical basis for similarity and the corresponding scaling relationship are discussed based on the fingering criteria. Microfluidic experiments are performed in chips of two size using a sloping platform. Gravitational condition and injection rate are designed based on the derived scaling relationship to validate the similarity of displacement process. Flow behaviours of the prototype and the scaled-down model are compared from the aspect of flow pattern, displacement efficiency, and breakthrough time.

2 THEORETICAL BASIS

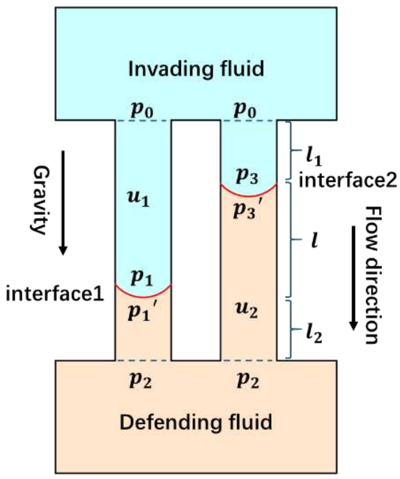

Figure 1. The sketch of theoretical bi-channel model. The two-phase interface was marked by red line. (Wang et al., 2025)

According to the two-dimension bi-channel model (Figure 1), the ratio of quasi-steady velocity in Channel 2 (u_2) and that in Channel 1 (u_1) can be calculated according to Eq.(1) (Wang et al., 2025):

$$\frac{u_2}{u_1} = 1 + \frac{\frac{c}{r^2}(\mu_i - \mu_d)l - \frac{1}{u_1}\left\{gl(\rho_i - \rho_d) - \sigma\kappa_1 + \sigma\kappa_2 - [2\rho_i l_1 + 2\rho_d l_2 + (\rho_i + \rho_d)l]\frac{\partial u_1}{\partial t}\right\}}{\frac{c}{r^2}\left(\mu_i l_1 + \mu_d(l_2 + l)\right) + u_0(\rho_i - \rho_d)} \quad (1)$$

where σ is surface tension coefficient; ρ_i, ρ_d are the density of invading and defending fluid; μ_i, μ_d are the viscosity of invading and defending fluid, r is the width of channels (characteristic size), κ_1, κ_2 are the curvature of the meniscus in Channel 1 and Channel 2, c is a constant, g is gravitational acceleration (taking positive when the direction of displacement is the same as gravity). Fingering occurred when $u_1 > u_2$, and the criterium for fingering occurrence can be obtained from Eq.(1) based on the typically low Reynolds number for microfluidic flow in porous media ($\rho u \ll \mu/r$):

$$\frac{\mu_i}{\mu_d} + \frac{(\rho_d - \rho_i)gr^2}{c\mu_d u_1} + \frac{\sigma(\kappa_1 - \kappa_2)r^2}{c\mu_d u_1 l} < 1 \quad (2)$$

The first term in the left-hand side of Eq.(2) represents the influence of viscosity, while the second term shows the effect of gravity. The third term represents the influence of capillary force, and the last one is the term of inertia. When the terms in criteria remain unchanged, the flow behaviour should remain consistent despite the variation of specific parameters. This also constitutes the necessary and sufficient condition for maintaining the three vital dimensionless number (viscous ratio $M = \mu_i/\mu_d$, capillary number $Ca = \mu_i v/\sigma$, and bond number $B_m = n(\rho_i - \rho_d)gr^2/\sigma$) unchanged, thus ensuring the same location in the three-dimension phase diagram proposed by Wang et al. (2025). Based on this, experiments can be designed adhering to similarity by varying alternative parameters, enabling investigation of phenomenon influenced by parameters unable or inconvenient to change. Specifically, the large-scale or long-duration displacement behaviours can be accelerated to an observable timescale by a downscaled model under hypergravity. For example, the phenomenon under normal gravity could be replicated by a 1/n scaled model under n^2 scaled gravitational acceleration with characteristic velocity unchanged (where n is the scaling parameter), under which circumstance the terms in fingering criteria maintains unchanged. And the process is accelerated by a factor of n, because the dimensionless characteristic time ($T = r/u$, where r is the characteristic size and u is the characteristic velocity) scales to $1/n$ of its value in the prototype when the characteristic size is downscaled by a factor of n and the characteristic velocity remains unchanged.

3 MATERIALS AND METHODS

To investigate the similarity of two-phase displacement under gravitational effect, microfluidic experiments were performed using a sloping platform. PDMS chips with uniformly arranged disks were fabricated as the 2D porous medium (with depth of 70 μm) for two-phase displacement experiments. The specific size of prototype and downscaled model are detailed in Figure 2. To acquire a large density difference between the two phases and thereby amplify gravitational effects, water stained by a 0.01% addition of Erioglaucine Disodium Salt (dynamic viscosity 1.68×10^{-3} Pa·s, density 1×10^{-3} kg/m^3) was used as invading fluid, while air (dynamic viscosity 1.813×10^{-5} Pa·s, density 1.2×10^{-6} kg/m^3) serves as defending fluid. Surface tension and contact angle were determined to be 74.13 mN/m and 110.4° (hydrophobic), respectively, using a video-based contact angle goniometer (Dataphysics OCA 20)—via the pendant drop method (for surface tension) and sessile drop method (for contact angle).

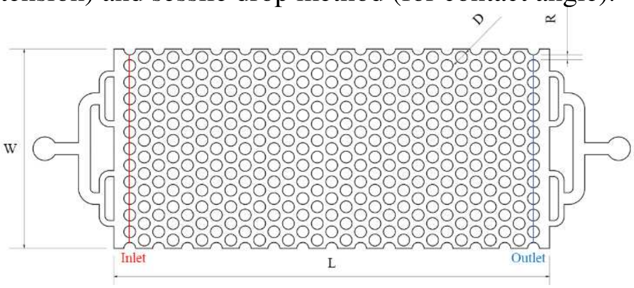

	Prototype (Chip 1)	Downscaled model (Chip 2)
D (mm)	1	0.5
R (mm)	0.414	0.207

L (mm)	37	19.5
W (mm)	16.968	8.484

Figure 2. The sketch of chips used for experiments, and the corresponding geometric dimensions of the prototype and downscaled model.

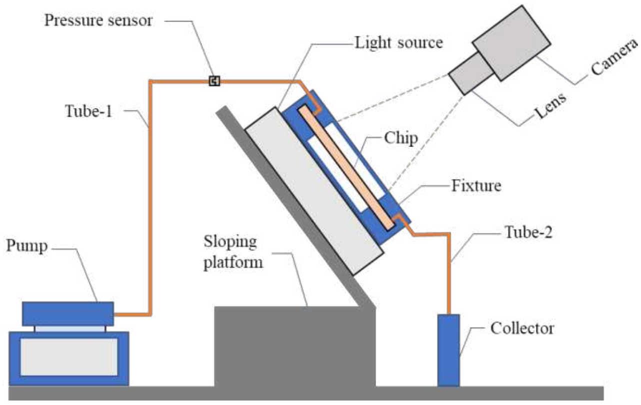

Figure 3. The sketch of experiments apparatus.

During experiments, PDMS chip was held in the fixture (with a 30mm×30mm hollow area) perpendicular to the bottom plate, which was connected to the Micro Syringe Pump (PHD Ultra Syringe pump Harvard) for fluid injection as shown in Figure 3. Digital camera (Alpha 7S3, Sony) and lens (FE 90mm F2.8 Macro G OSS) were placed parallel to the fixture to perform high quality video recording during displacement (with a maximum image resolution of 4096×2160 at 120 fps, and a shutter speed minimum to 250μs). In order to improve the recording quality, a surface light source was placed behind chip fixture to reduce exposure time and eliminate the interference from ambient light.

Prior to each experiment, air is injected through Tube 1 and Tube 2 into the unloaded chip fixture using syringes, ensuring the absence of residual clusters. A microfluidic chip is then mounted into the fixture, and the slope angle is adjusted as required. The camera is configured with appropriate parameters and focused to guarantee clear imaging of the porous medium structure on the chip. Subsequently, the experimental fluid is injected at a flow rate of 20 μL/min via a syringe pump; injection is paused once the fluid interface reaches the inlet of the fixture. After the pressure stabilizes, the syringe pump flow rate is adjusted to the prescribed value, and fluid injection is initiated alongside synchronous data acquisition. Injection and data recording are terminated after a cumulative injection of 2 pore volumes (2 PV). The microfluidic chip is then disassembled, and the procedure is repeated from the initial step for the next experimental run. The specific setting of injection rate and slop angle are designed orthogonally according to the scaling relationship, as detailed in Table. 1.

Case	Chip	Injection Rate ($\mu l/min$)	Slope Angle (°)	Capillary Number	Bond Number
1	1	0.05	0	1.64×10^{-8}	0
2	1	0.05	14.48	1.64×10^{-8}	1.02×10^{-4}
3	1	0.05	90	1.64×10^{-8}	4.07×10^{-4}
4	1	20	0	6.55×10^{-6}	0
5	1	20	14.48	6.55×10^{-6}	1.02×10^{-4}
6	1	20	90	6.55×10^{-6}	4.07×10^{-4}
7	2	0.025	0	1.64×10^{-8}	0
8	2	0.025	90	1.64×10^{-8}	1.02×10^{-4}
9	2	10	0	6.55×10^{-6}	0
10	2	10	90	6.55×10^{-6}	1.02×10^{-4}

Table.1 Experimental conditions and corresponding dimensionless numbers

4 RESULTS AND DISCUSSION

4.1 Influence of gravity

The situation in experiments corresponds to the scenario of gravitational instability and favorable viscosity ratios, indicating the competition of gravity and viscous force: the former promotes fingering while the latter inhibits it.

Given the denser invading fluid injected from top, gravity favors flow along gravitational acceleration direction which induces preferential flow and fingering, leading to the declination of displacement efficiency under low injection rate. As shown in Figure 4 (a), in the prototype, the invading fluid tends to protrude into defending fluid, leading to finger-like flow pattern, especially under low injection rate. Under the injection rate of 0.05 μl/min (Ca of 1.64×10^{-8}), the relative compact flow pattern in the absence of gravitational effects (Bo = 0) transits to preferential flow characterized by narrow fingering of invading fluid as gravitational acceleration increases to 1g (Bo = 4.07×10^{-4}), inducing a decrease of 30.24% in saturation of invading fluid. However, the influence of gravitational effect on flow pattern gets less obvious with rise of injection rate. Under the injection rate of 20 μl/min, a compact flow pattern is maintained under all gravitational condition (0g and 1g), with saturation of invading fluid fluctuating around 85.23% (maximum deviation of ±4%). This trend stems from the competition between viscous force and gravity. While gravity applies a sharper hydrostatic pressure in the more denser invading fluid which enlarges the pressure difference between phases at the leading menisci and promotes fingering, the viscous force does the opposite for the more severe viscous dissipation in invading fluid compared with that in defending fluid. This is also reflected by the fingering criteria (Eq. (2)), the gravitational term is negative when invading fluid is denser ($\rho_d - \rho_i < 0$) and flows downward ($g > 0$), while the viscous term is positive when invading fluid is more viscous ($\mu_i - \mu_d > 0$). As a result, the fingering pattern induced by gravity is suppressed with the increase of injection rate.

Similar trend is observed in the downscaled model: gravity decreases saturation of invading fluid on breakthrough for over 10.22% under low injection rate with capillary number below 1.64×10^{-7}, while exert limited influence (less than 5%) under the capillary number of 6.55×10^{-6}. Additionally, the gravitational effect is less pronounced in the downscaled model. As shown in Figure 4 (b), the decrease in it is much smaller than that in the prototype. Given the displacement efficiency under zero gravity (Bo = 0) close to that in prototype, the downscaled model presents a relatively more stable pattern with higher displacement efficiency. This reveals the influence of characteristic dimension (width of throat) to gravitational effect. As indicated by Eq. (2), the gravitational term in fingering criteria is proportional to the square of characteristic dimension. Thus, the absolute value of gravitational term is decreased when the model is downscaled, resulting in the less pronounced outcome of gravitational effect.

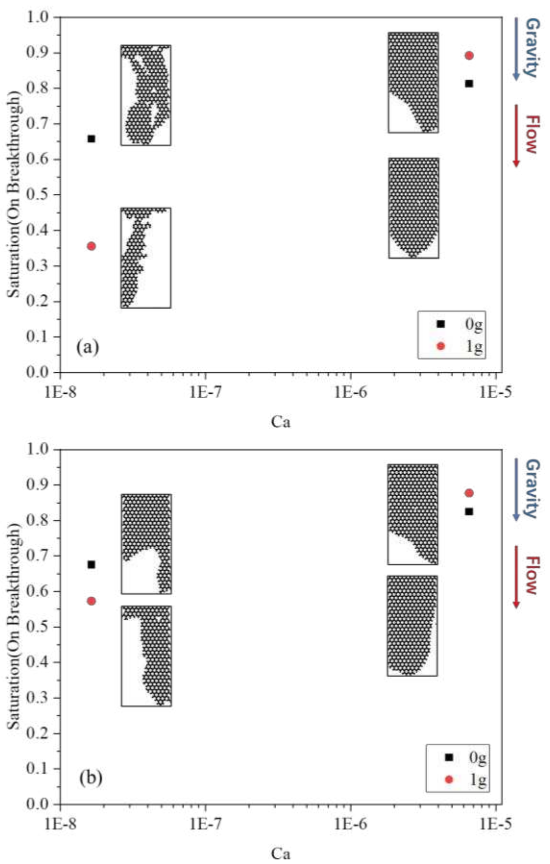

Figure 4. Two phase distribution on breakthrough and the corresponding saturation of invading fluid with gravitational acceleration varying from 0 to 1g in (a) chip of prototype and (b) chip of downscaled model

4.2 Validation of similarity

To validate the similarity of two-phase displacement patterns under gravitational effects, the flow characteristics of the prototype are compared with those of the downscaled model—where experiments are conducted under the same dimensionless numbers in accordance with the scaling relationships.

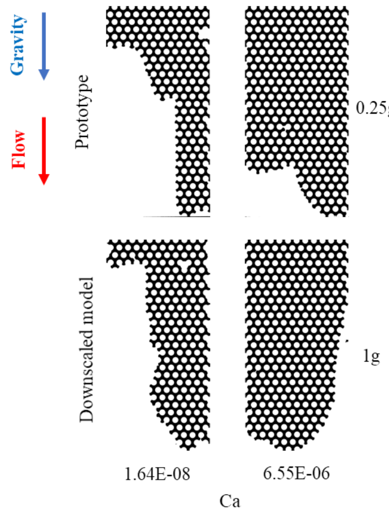

Figure 5. Two phase distribution on breakthrough in prototype and downscaled model with Bo of 1.02×10^{-4} *and Ca of* 1.64×10^{-8} *and* 6.55×10^{-6}.

4.2.1 Flow pattern

With dimension downscaled to half of the prototype and effective gravitational acceleration enlarged to 400% that of prototype, the two phase distribution on breakthrough in the downscaled mode remain almost consistent with that in prototype while Ca increases from 1.64×10^{-8} to 6.55×10^{-6}. As shown in Figure 5, preferential flow developed beside the boundary under low injection rate with Ca of 1.64×10^{-8}, manifesting the influence of capillary force and gravity. With the increasing of injection rate and the rise of Ca, the pattern transitions in prototype and downscaled model remain synchronously. When Ca reaches 6.55×10^{-6}, the protruding of invading fluid is not obvious in both prototype and downscaled model, and fingering or preferential flow is not observed.

4.2.2 Saturation and fractal dimension

The saturation of invading fluid on breakthrough in both prototype and downscaled model demonstrates an increase over 30% as Ca rises from

1.64×10^{-8} to 6.55×10^{-6}, as shown in Figure 6 (a). Meanwhile, this saturation in prototype and downscaled model remains close under the same Ca, with the average deviation of 3.98%. The fractal dimension (an index measured by box count method to account for the complexity of invading-fluid boundary) of the two models (prototype and downscaled version) also exhibit consistent variation: the average relative deviation of fractal dimension under the same capillary number (Ca) is only 0.02 as shown in Figure 6 (b). The consistent evolution of saturation and fractal dimension further validate similarity.

Although there is overall consistency in the general pattern, certain discrepancies still exist. The two phase interface in the prototype is more irregular compared with that in the downscaled model as shown in Figure 5, companied with a lower saturation of invading fluid on breakthrough as shown in Figure 6 (a). These discrepancies may origins from the interference of inertial effects, which is omitted under the low-Re assumption in theoretical analysis.

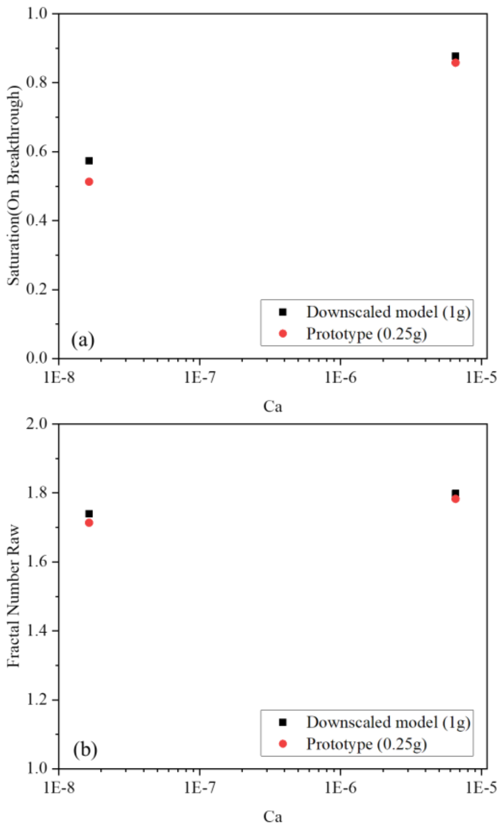

Figure 6. (a) The saturation of invading fluid on breakthrough and (b) the corresponding fractal dimension in prototype and downscaled model with Bo of 1.02×10^{-4}.

4.2.3 Breakthrough time

The breakthrough time—the time at which the invading fluid reaches the final row of pillars—exhibits a non-linear decrease with increasing injection rate (i.e., increasing capillary number, Ca). While this trend cannot be precisely fitted by an inverse proportion function due to the pattern transition, the proportion of declination in prototype and downscaled model remains consistent. As shown in Figure 7 (a), when injection rate increased by 400 times with Ca increasing from 1.64×10^{-8} to 6.55×10^{-6}, the breakthrough time is shortened to 0.3617% and 0.3937% of the original in prototype and downscaled model respectively. The average deviation of this declination between them is as low as 1.6%, revealing the consistency of dynamics between prototype and downscaled model.

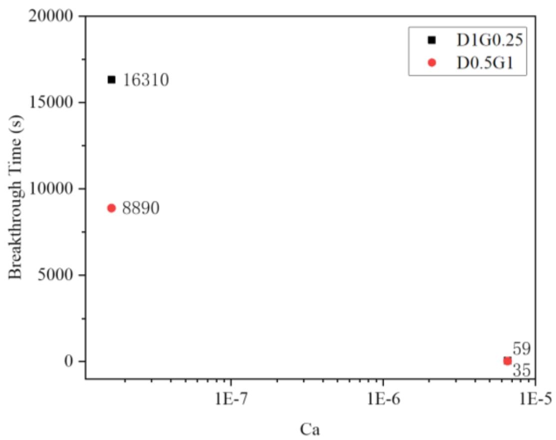

Figure 7. The break through time versus capillary number (Ca) in prototype and downscaled model with Bo of 1.02×10^{-4}.

Additionally, at the same flow velocity (Ca), the breakthrough time of displacement in the 0.5× downscaled model is shorter, approximating half of that in the prototype, confirming a near-ideal 0.5:1 scaling relationship for breakthrough time between the downscaled model and the prototype. This agrees with the scaling relationship derived from theoretical analysis, that the displacement is speeded up for n times in the 1/n downscaled model with gravitational acceleration magnified by n^2.

5 CONCLUSION

Gravitational effects and the similarity scaling principles of two-phase displacement were investigated via microfluidic experiments, with flow behaviors and corresponding mechanisms analyzed. Conclusions are summarized as follows: 1) A scaling relationship for displacement pattern similarity is proposed, based on the analysis of theoretical fingering criteria and phase diagrams. Specifically, in a 1/n downscaled model under n² amplified gravitational acceleration, the dimensionless numbers (Ca, M, B_m) remain identical, and a similar flow pattern is preserved. 2) Gravitational effects exert a non-negligible influence in experiments: when the invading fluid is denser and displacement occurs in the top-to-bottom direction, gravity promotes fingering and preferential flow. This influence, however, is suppressed under high flow rates or in scaled-down porous media due to the amplification of viscous force and capillary force. 3) Experiments conducted in accordance with the proposed similarity scaling relationship reveal that flow patterns, displacement efficiency, and fractal dimensions are consistent between the prototype and down scaled model. Breakthrough time, by contrast, follows a 1/n scaling law. This cross-model consistency provides evidence for the validity of the similarity scaling principle. This work elucidates the regularity of gravitational similarity of two-phase displacement processes, and offers insights for scaling modeling in centrifugal experiments.

REFERENCES

Almajid, M. M., & Abu-Al-Saud, M. O. (2022). Prediction of porous media fluid flow using physics informed neural networks. Journal of Petroleum Science and Engineering, 208, 109205. https://doi.org/10.1016/j.petrol.2021.109205

Condie, S. A., & Rhines, P. B. (1994). A convective model for the zonal jets in the atmospheres of Jupiter and Saturn. Nature, 367(6465), 711–713. https://doi.org/10.1038/367711a0

Cui, G., Liu, M., Dai, W., & Gan, Y. (2019). Pore-scale modelling of gravity-driven drainage in disordered porous media. International Journal of Multiphase Flow, 114, 19–27. https://doi.org/10.1016/j.ijmultiphaseflow.2019.02.001

Dai, S., & Santamarina, J. C. (2017). Stiffness Evolution in Frozen Sands Subjected to Stress Changes. Journal of Geotechnical and Geoenvironmental Engineering, 143(9), 04017042. https://doi.org/10.1061/(ASCE)GT.1943-5606.0001713

Ewing, R. P., & Berkowitz, B. (1998). A generalized growth model for simulating initial migration of dense non-aqueous phase liquids. Water Resources Research, 34(4), 611–622. https://doi.org/10.1029/97WR03754

Girolami, L., & Risso, F. (2020). Physical modeling of the dam-break flow of sedimenting suspensions. Physical Review Fluids, 5(8), 084306. https://doi.org/10.1103/PhysRevFluids.5.084306

Golmohammadi, S., Ding, Y., Kuechler, M., Reuter, D., Schlueter, S., Amro, M., & Geistlinger, H. (2021). Impact of Wettability and Gravity on Fluid Displacement and Trapping in Representative 2D Micromodels of Porous Media (2D Sand Analogs). Water Resources Research, 57(10). https://doi.org/10.1029/2021WR029908

Hawlader, B. C., Muhunthan, B., & Imai, G. (2008). State-dependent constitutive model and numerical solution of self-weight consolidation. Géotechnique, 58(2), 133–141. https://doi.org/10.1680/geot.2008.58.2.133

Jung, J. W., Jang, J., Santamarina, J. C., Tsouris, C., Phelps, T. J., & Rawn, C. J. (2012). Gas Production from Hydrate-Bearing Sediments: The Role of Fine Particles. Energy & Fuels, 26(1), 480–487. https://doi.org/10.1021/ef101651b

Løvoll, G., Méheust, Y., Måløy, K. J., Aker, E., & Schmittbuhl, J. (2005). Competition of gravity, capillary and viscous forces during drainage in a two-dimensional porous medium, a pore scale study. Energy, Second International Onsager Conference, 30(6), 861–872. https://doi.org/10.1016/j.energy.2004.03.100

Rücker, M., Berg, S., Armstrong, R. T., Georgiadis, A., Ott, H., Schwing, A., Neiteler, R., Brussee, N., Makurat, A., Leu, L., Wolf, M., Khan, F., Enzmann, F., & Kersten, M. (2015). From connected pathway flow to ganglion dynamics. Geophysical Research Letters, 42(10), 3888–3894. https://doi.org/10.1002/2015GL064007

Thring, M. W. (1953). Eddies in Turbulent Jet Diffusion Flames. Nature, 172(4379), 634–635. https://doi.org/10.1038/172634a0

Tong, X., Wang, Z., Cheng, Z., Zhou, C., & Mao, N. (2017). A modeling method for predicting the concentration of indoor carbon dioxide leakage and dispersion based on similarity theory. Energy and Buildings, 151, 585–591. https://doi.org/10.1016/j.enbuild.2017.07.001

Wang, L., Zuo, X., Liu, H., Yue, T., Jia, X., & You, J. (2019). Flying qualities evaluation criteria design for scaled-model aircraft based on similarity theory. Aerospace Science and Technology, 90, 209–221. https://doi.org/10.1016/j.ast.2019.04.032

Wang, Liu, Pengfei., Chen, Kexin., Chen, Yunmin., & Bate, B. (2025). Hypergravity effects on immiscible two-phase displacement processes via CFD simulation and an analytical bi-channel model. Computers and Geotechnics, 186, 107417. https://doi.org/10.1016/j.compgeo.2025.107417

Zhou, J., Zhou, Y., Yang, Z., Wei, C., Wei, H., & Yan, R. (2021). Dissociation-Induced Deformation of Hydrate-Bearing Silty Sand During Depressurization Under Constant Effective Stress. Geophysical Research Letters, 48(14), e2021GL092860. https://doi.org/10.1029/2021GL092860